RSC Advances

ROYAL SOCIETY OF CHEMISTRY

www.rsc.org/advances

Bifunctional graphene oxide-cellulose nanofibril aerogel loaded with Fe(III) for removal of cationic dye via simultaneous adsorption and Fenton oxidation

Mohd Shaiful Sajab [a,b,*], Chin Hua Chia [a,*], Chi Hoong Chan [a], Sarani Zakaria [a], Hatika Kaco [a], Soon Wei Chook [a], Siew Xian Chin [a], An'Amt Mohamed Noor [c]

[a] *Bioresources and Biorefinery Laboratory, School of Applied Physics, Faculty of Science and Technology, Universiti Kebangsaan Malaysia, 43600 Bangi, Selangor, Malaysia*

[b] *Research Center for Sustainable Process Technology (CESPRO), Faculty of Engineering and Built Environment, Universiti Kebangsaan Malaysia, 43600 Bangi, Selangor, Malaysia*

[c] *Fakulti Agro Industri dan Sumber Asli, Universiti Malaysia Kelantan, Karung Berkunci 36, Pengkalan Chepa, 16100 Kota Bharu, Kelantan, Malaysia*

* Corresponding author. Tel: +603 8921 5473. Fax: +603 8921 3777.

E-mail: mohdshaiful@ukm.edu.my (M.S. Sajab); chia@ukm.edu.my (C.H. Chia)

ABSTRACT

A highly porous cellulose nanofibril (CNF) aerogel loaded graphene oxide with iron (III) (GO-Fe) nanocomposites was produced and used for the treatment of methylene blue (MB) aqueous solution. The CNF serves as an adsorbent for the dye, while the GO-Fe nanocomposites play a role in the decomposition of the dye via the Fenton oxidation reaction. The aerogel exhibits rapid adsorption performance (less than 10 min.) in removing MB, with a maximum adsorption capacity of 142.3 mg/g. On the side of enhancing the MB removal, GO on the GO-CNF nanocomposite aerogel was loaded with 1 wt. % of Fe(III) content to perform as a catalyst for the Fenton oxidation reaction. The concentration of MB continues to decolorize for 30.4% more after 24h of reaction process. Moreover, by performing Fenton oxidation for adsorbent regeneration, the adsorption capacity for nanocomposite adsorption was reduced by 52.2% after five cycles of adsorption-oxidation.

Keywords: Cellulose nanofibrils; Fenton oxidation; Graphene oxide; Nanocomposite; Rapid adsorption; Regeneration

1. Introduction

Recent promising developments of various techniques used in wastewater treatment has witnessed an improvement in treatment efficiency and overcoming limitations as compared to conventional methods. An adsorption technique, for example, in the utilization of low-cost adsorbents was seamlessly developed to overcome the high-cost production of activated carbon.[1,2] The cost of adsorbent production is not only factor involved in developing an excellent adsorbent, there's also adsorption performance, regeneration ability and adsorbent segregation. The massive quantities and continuous discharge of industrial effluents requires an attentive, rapid and efficient solution for effluent treatment. Thus, there are a variety of micro- to nano-sized adsorbents from different materials were previously investigated to achieve rapid removal of wastewater effluents; e.g., modified activated carbon,[3] nano-sized metal oxides,[4] alumina nanoparticles,[5] mesoporous silica,[6] cellulose nanofibrils (CNF).[7]

Cellulose, a sustainable resource that can be extracted from lignocellulosic biomass, has been widely used in many forms of applications and products as it is a relatively stable polymer with high axial stiffness and high crystallinity, especially in the forms of micro- to nano-sized fibrillated cellulose.[8,9] CNF refers to defibrillated wood pulp by physical means with chemical, enzymatic or physical pre-treatments.[10,11] Therefore, in order to produce CNF, mechanical and physical disintegration is required. Various methods have been employed to defibrillate cellulose; e.g., a blender,[12] high-pressure homogenization,[13] steam explosion[14] and grinding.[15] CNF has many potential applications, such as a reinforcement in

composites,[16] thickening agent,[17] substrate for electronic devices,[18] scaffold for tissue growth,[19] cationic dye adsorbent,[7] etc.

In recent years, the research on graphene-based materials in various fields of applications has grown, blossoming mainly due to its exceptional physical and electronic characteristics.[20] Among them is graphene oxide, modified graphene sheets with a large number of reactive oxygen functional groups (hydroxyl, epoxy, carbonyl and carboxyl). These advantages contribute to strong electrostatic interactions and the hydrophilicity of the large, surface area GO. The large surface area and great number of oxygen atoms on GO produces strong electrostatic interactions.[21,22,23] These factors help GO possess a high adsorption capacity against cationic dyes in aqueous solutions, comparable to the commercial-activated carbon.[24] However, its extremely small size and hydrophilicity has limited the practical applications in wastewater treatment, which requires an additional step of centrifugation for the recollection of the GO from the treated effluent.[25] To overcome the separation difficulties, several approaches have been adopted, including the formation of hydrogel,[26] aerogel,[27] encapsulation[28,29,30] functionalization of magnetic nanoparticles.[31,32]

In our previous study, CNF and GO proved to be efficient and promising adsorbents for the rapid removal of cationic dye.[7,24] Therefore, in the present work, GO was immobilized in CNF aerogel and used to remove methylene blue from aqueous solution. Furthermore, in order to enhance the efficiency for dye removal, GO was loaded with Fe(III) ions to assist in the removal of MB by Fenton oxidation reaction after the adsorption process of the aerogel. The adsorption performances (adsorption kinetics, maximum adsorption capacity, regeneration) of the aerogel with different GO contents were investigated.

2. Experiment

2.1 Materials

Kenaf core (KC) powder was obtained from the Malaysia Agricultural Research and Development Institute (MARDI), and sodium chlorite, 80% (Acros Organics), and glacial acetic acid, 95% (R&M Chemicals), were used for preparation of CNF. GO was prepared by using graphite flakes (Ashbury, Inc. USA), phosphoric acid, 85% (Merck), potassium permanganate, 99.9% (Merck), hydrogen peroxide, 30% (Merck) and ferric chloride (Systerm). Stock solutions of methylene blue (MB) trihydrate (Sigma-Aldrich) were prepared and diluted accordingly. Standard calibration of diluted MB solutions was measured using a UV-Vis spectrophotometer (Jenway 7315 Spectrophotometer) at a λ_{max} of 664 nm.

2.2. Preparation of GO-CNF nanocomposite aerogel

CNF was prepared from KC wood powder according to a previous study.[7] Briefly, KC powder was rinsed several times with distilled water to remove impurities and delignified six times through acid-chlorite bleaching to obtain holocellulose (total of 1.875 g/g of sodium chlorite and 1.25 g/g of acetic acid). Defibrillation of the holocellulose was performed using a high-speed blender (Vitamix, Vita-Prep 3) at 0.7 wt.% consistency of holocellulose and 0.1 mM of NaCl as a counter ion. The defibrillation process was carried out for 30 minutes. The produced CNF was stored at 4°C in a refrigerator for further use.

GO used in this study was prepared using Hummer's method.[24] To start the oxidation process, whereby a mixture of H_2SO_4 (360 mL), H_3PO_4 (40 mL), $KMnO_4$ (18 g) and graphite flakes (3 g) was stirred for three days. Next, the solution was mixed with ice (400 mL) and H_2O_2 (27 mL) to stop the oxidation process. The solution was washed with HCl (1 M) three times and deionized water ten times until the pH of the solution reached pH 4-5. The produced GO suspension was added to 0.01 g ferric chloride ($FeCl_3$), which is the equivalent of 1.0 wt% Fe(III), and stirred for 60 minutes to produce GO-Fe nanocomposites. The desired

volume of GO-Fe was added into a beaker containing 20 mL CNF suspension (5 wt.%). The mixture was stirred at room temperature for 30 minutes using a magnetic stirrer. The mixture was lyophilized in a freeze-dryer (brand model) for 24 hours to form aerogel. The produced aerogels were kept in desiccator for further uses. Aerogels with different percentages of GO-Fe (5, 10, 15, 20 and 30 wt.%) were produced. Besides, CNF and GO aerogels were also prepared as control samples using the same procedure.

2.2 Characterizations of GO-CNF nanocomposite

The nanocomposites (CNF and GO-CNF) were analyzed using a transmission electron microscopy (TEM) (CM 12 Phillips). The sample was diluted using ethanol (ca. 0.01 wt.%) and dropped onto a copper grid and stained with uranyl acetate (3 wt.%). Attenuated total reflectance Fourier transform infrared spectroscopy (ATR-FTIR) (Perkin-Elmer Spectrum 400) characterization for the functional groups of freeze-dried samples (GO, CNF, and GO-CNF) was performed in the resolution of 1 cm^{-1} in the range of 4000 cm^{-1} to 650 cm^{-1}.

2.3 Adsorption experiments

2.3.1 Adsorption kinetics

Adsorption kinetic experiments were conducted in a flask containing 100 mL of MB solution at different concentrations. The initial pH of the dye solutions was fixed at 7 according to a previous study.[7] The mixture was stirred at a constant speed of 250 rpm with a magnetic stirrer for 2 hours until equilibrium was achieved. Aliquots of solution (~0.1 mL) were withdrawn at different time intervals, filtered using nylon-membrane syringe filter (Agilent, 0.2 μm), diluted using deionized water, and analyzed using a UV-vis spectrophotometer. The concentration of dye adsorbed at time t, q_t (mg/g), was calculated using following equation:

$$q_t = \frac{(C_0 - C_t)V}{m} \quad (1)$$

where C_0 and C_e are the initial and equilibrium concentrations of dye solution (mg/L), respectively. V is the volume of the solution (mL) and m is the mass of the adsorbent (g). Adsorption kinetics data was fitted to the pseudo-second order,[33] where k_2 (g/mg min) is the rate constant of pseudo-second order expressed as below:

$$q_t = \frac{k_2 q_e^2 t}{1 + k_2 q_e t} \quad (2)$$

2.3.2 Adsorption isotherms

Adsorption isotherm was performed in a series of MB concentrations (50, 100, 200, 300, 400, 500 and 600 mg/L) at room temperature. The mixture of 25 mL of MB solution and 0.025 g of nanocomposite aerogel adsorbents was placed in a rotary shaker at a constant speed of 200 rpm for 2 hours. The final concentration of MB solution (C_e) at equilibrium was measured using the spectrophotometer to calculate the amount of adsorbed MB at equilibrium (q_e) using the following equation:

$$q_e = \frac{(C_0 - C_e)V}{m} \quad (3)$$

2.4 Simultaneous adsorption-Fenton oxidation

A similar procedure of adsorption kinetics experiments was performed with an additional 40 mM of H_2O_2 in the MB solution as an oxidizing agent. The mixture was stirred at a constant speed of 250 rpm with a magnetic stirrer for 24 hours or until equilibrium was achieved.

2.5 Regeneration studies

Adsorption was done using 100 mg/L MB (100 mg/L) for 2 hours to achieve adsorption saturation. The adsorbent was washed with deionized water to remove excessive MB. Fenton oxidation was carried out by mixing the washed adsorbent with 25 mL of 40 mM H_2O_2 for 24

hours. The adsorbent was again washed with deionized water to remove excessive H_2O_2. Regeneration of the nanocomposite adsorbents was performed for five cycles (adsorption-Fenton oxidation) using a similar procedure (100 mg/L MB solution) at room temperature.

3. Results and discussion

3.1 Characterizations of nanocomposite

The fibrillation process on the KC powder shows the aggregated CNF with nano diameter sizes under TEM images (see Fig. 1(a)). Similar with the previous report on KC CNF,[7] the diameter of individual nanofibrils observed is in the range of 3.3-8.9 nm, with the average being 5.9 nm. On the other hand, the TEM images of the GO-CNF suspension shows a thin layer of GO was noticeably deposited on a web-like structure of CNF (see Fig. 1(b)). The tips of the GO layer were ripped and grafted on the CNF, which is shown in a higher magnification of TEM images (inset of Fig. 1(b)). In the suspension form, both GO and CNF interact with each other via intermolecular hydrogen bonding that allowed a homogeneous alignment/connection between the nanocellulose and GO. Additionally, the interaction between GO-CNF prevents the GO layers from over-stacking and retaining their active surface sites.[22,23]

The morphology and structure of the CNF and GO-CNF aerogel nanocomposite were shown in Fig 1(c) and (d), respectively. As shown in Fig. 1(c), the CNF aerogel exhibited a highly porous structure, which was likely formed throughout the freeze drying process. The intermolecular hydrogen bonding among CNF led to an entanglement of CNF, while the subsequent removal of water molecules resulted in the porous structure of the CNF foam.[34] Additionally, the SEM images of the GO-CNF nanocomposite exhibited a more porous structure, which is mainly due to the presence of GO. A three-dimensional (3-D) network was possibly formed out of these interactions between GO-CNF and GO-GO.[35] The additional

GO has been attributed to a crosslinking effect with CNF due to the intermolecular hydrogen bonding between cellulose and GO.[22,36] However, the presence of Fe within the nanocomposite is hardly to be identified by taking into consideration the small amount of Fe(III) that was added.

FTIR spectra of CNF nanocomposite (see Fig. 2), show all characteristic peaks for cellulose (3341, 2915, 1640 and 1160 cm^{-1}), which is attributed from the O−H stretching, aliphatic alkyls stretching, adsorbed water and ether linkages of pyranose, respectively.[7] IR spectra on GO showed characteristic peaks at 1391 and 1737 cm^{-1} are due to C−O−H deformation and C=O stretching of COOH groups, respectively. The absorption bands at 1072 and 1249 cm^{-1} are due to the epoxy ring deformation and C−O stretching mixed with C−OH bending, respectively.[24] Both GO/GO-Fe-CNF nanocomposites have introduced peak at 1419, 1621 and 1719 cm^{-1}, which can be attributed to vibration of O−H, intramolecular hydrogen bonds and the surface functionality of GO and CNF, respectively.[22]

A loading with a 100 g of weight was placed on top of the GO, CNF and GO-CNF aerogels to investigate their compression properties. GO aerogel, a low-density material, is likely to have low mechanical property and can be compressed easily under a 100 g of mass (see Fig. 3). Meanwhile, GO-Fe-CNF nanocomposite shows a good mechanical property and maintained its aerogel structure before and after the compression (see Fig. 3). The good mechanical properties of CNF aerogel (flexibility and ductility) are attributed to the strong intermolecular hydrogen bonds and the highly porous structure of CNF during the drying process.[34] Therefore, CNF has constructed a good mechanical structure with the incorporation of GO to prevent the deformation of the aerogel.

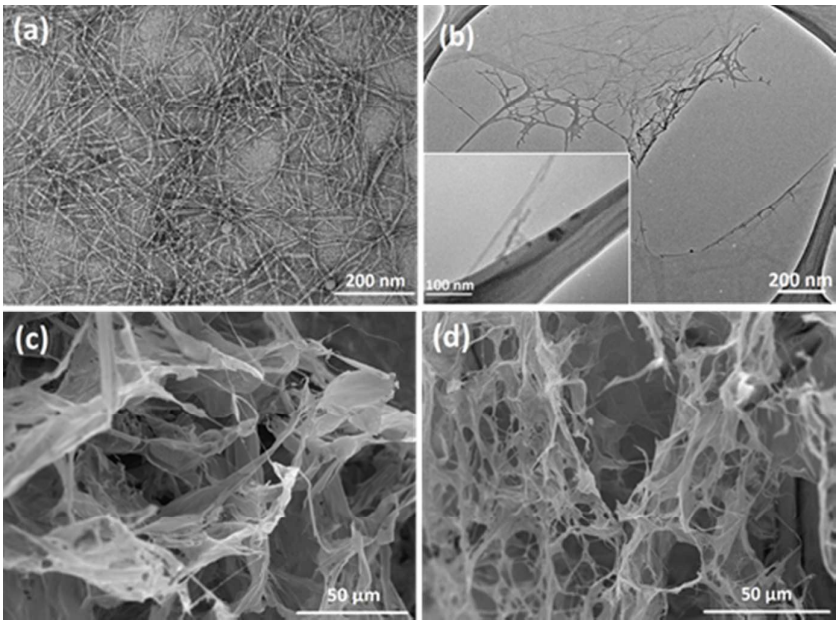

Figure 1 Morphology images of nanocomposite suspension from TEM for (a) CNF and (b) 20%GO-Fe-CNF and aerogel from SEM for (c) CNF and (d) 20%GO-Fe-CNF

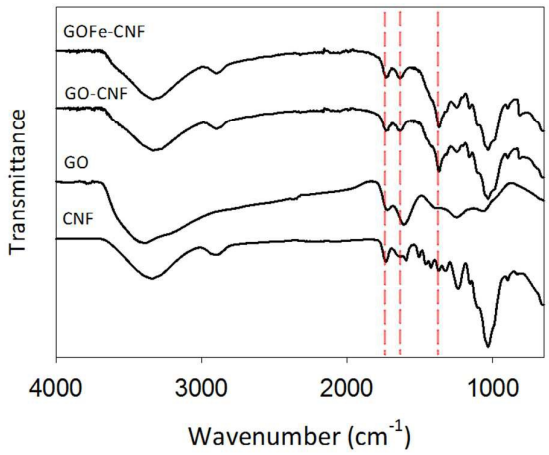

Figure 2 Characterizations of nanocomposites (CNF, 20%GO-CNF and 20%GO-Fe-CNF) for FT-IR spectra

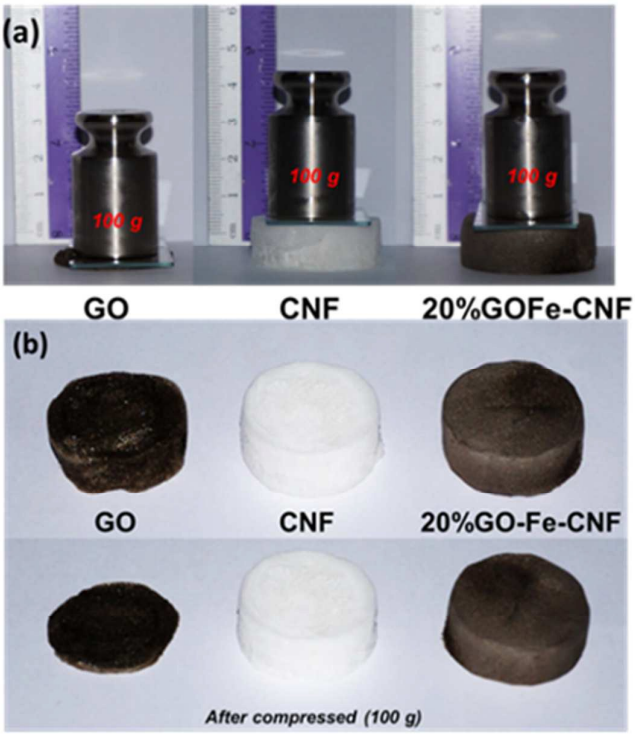

Figure 3 Compression of (a) GO, CNF and 20%GO-Fe-CNF in nanocomposites aerogel using 100 g mass and (b) comparison after aerogel has been compressed

3.2 Rapid adsorption of GO-CNF nanocomposite

GO possesses high surface functionalities (hydroxyl, carboxyl, carbonyl, etc.) and a large specific area, which contributed to the high adsorption capacity and rapid adsorption.[24] As the GO suspension formed into GO aerogel via freeze drying, adsorption capacity reduced approximately 50% to 384 mg/g., which can be attributed to the decrease of total exposed surface of the GO (see Fig. S1).[28] The rapid adsorption kinetics of CNF aerogel for the removal of MB was acquired, and the adsorption equilibrium was achieved in less than 5 minutes (see Fig. 4(b)). CNF has a higher adsorption rate, k_2, compared to GO suspension, 0.0218 and 0.0007 g/mg min, respectively (see Table S1). The efficiency of CNF to rapidly uptake cationic dye has been reported in our earlier work.[7]

In order to obtain a better adsorption capability, GO suspension was used as a surface modifier on CNF to form a good nanocomposite adsorbent. By adding 5 wt. % of GO on CNF nanocomposite, its adsorption capacity was increased 16%, i.e., from 100.3 to 116.5 mg/g. The high specific surface area and chemical functional groups of both GO and CNF are the main reasons for the rapid adsorption performances of the nanocomposites. In addition, as can be seen in Fig. 1(d), the pore structure of the CNF nanocomposite was undisrupted by the addition of GO modification.

The adsorption capacity of GO was reduced significantly after loading with 1 wt.% of Fe(III), which is 28% lower than the GO (see Fig. S1). Moreover, a similar amount of Fe content was added onto the CNF and resulted in a much lower MB uptake (5.4 mg/g) (see Fig 4(a)). The reduced adsorption capacity of both GO and CNF can be attributed to the reduction of reactive sites due to being partially occupied by the Fe ions via electrostatic interaction.[37]

In order to identify the optimum parameter for GO-Fe-CNF nanocomposite, the amount of GO-Fe added onto CNF was increased accordingly (5, 10, 15, 20 and 30 wt.%) (see Fig. 4(c)). The adsorption capacity of the GO-Fe is much higher as compared to CNF, therefore, it is expected that the increasing amount of GO-Fe in CNF will boost its adsorption capacity. 30%GO-Fe in CNF has increased the adsorption capacity up to 143 mg/g. However, the increment of GO-Fe content in the nanocomposite has prolonged the adsorption equilibrium time and decreased the adsorption rate, $k_{2,}$ from 0.0091 to 0.0036 g/mg min. This could be due to the fact that GO sheets overlay each other at high concentration, whereby lower GO content is favored for better interaction with CNF for preventing over stack of the GO layers [22, 23].

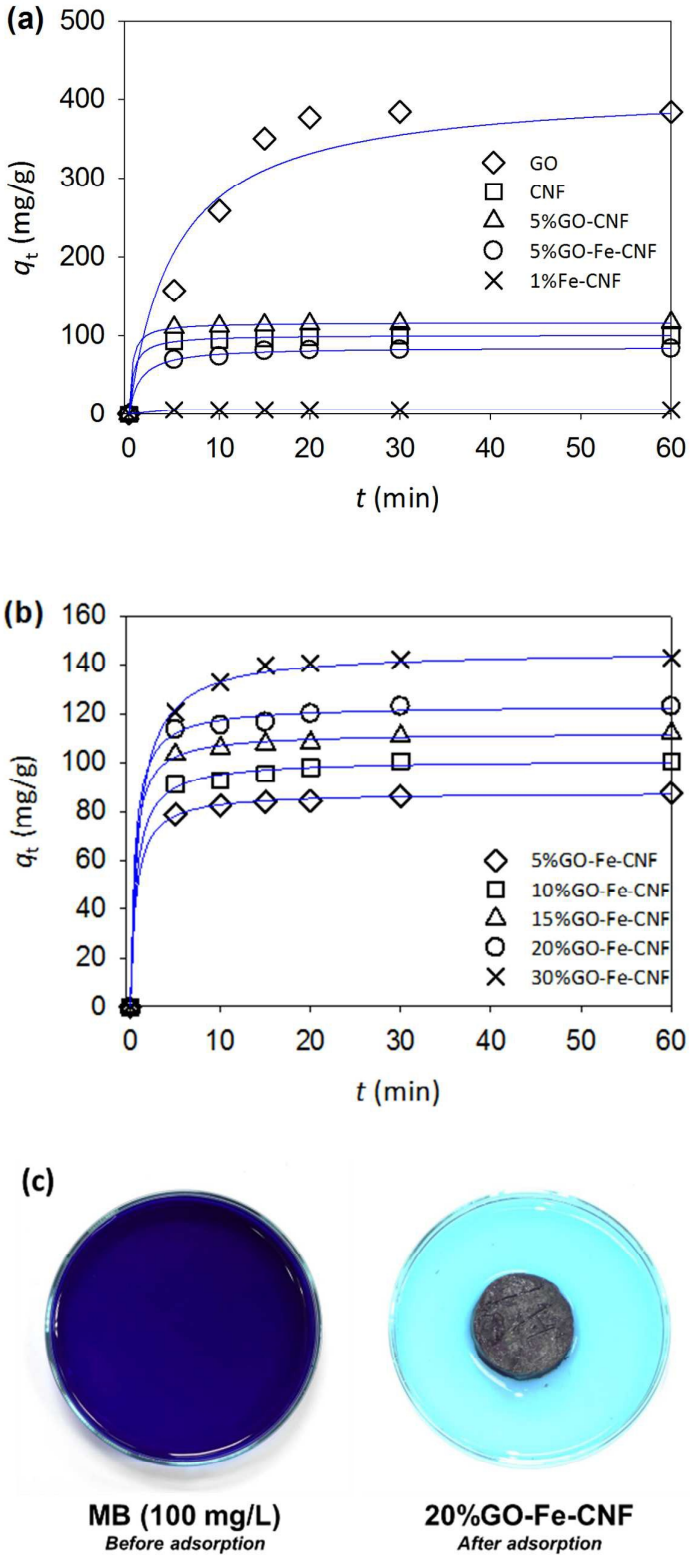

Figure 4 Adsorption kinetics of MB (600 mg/L) fitted to the pseudo-second order from (a) GO and CNF nanocomposite aerogels, (b) different wt.% of GO-Fe on CNF nanocomposites

and the image taken for (c) MB solution (100 mg/L) before and after 30 minutes of adsorption using 20%GO-Fe-CNF.

3.3 Adsorption isotherm

Briefly, the derivation of Langmuir assumed monolayer adsorption between the adsorbate molecules and adsorbent medium, while the Freundlich model explains the heterogeneous adsorption behavior of the adsorption mechanism. The Langmuir isotherm model can be expressed as:

$$q_e = \frac{Q_0 b C_e}{1 + b C_e} \tag{4}$$

where Q_0 is the maximum adsorption capacity per unit mass of adsorbent (mg/g) and b is a constant related to the adsorption energy (L/mg).[38] To determine whether adsorption is "favorable" or "unfavorable", a dimensionless constant separation factor or equilibrium parameter, R_L, was calculated using the following equation:

$$R_L = \frac{1}{1 + b C_m} \tag{5}$$

where b is the Langmuir constant (L/mg) and C_m is the highest initial MB concentration (mg/L). The value of R_L indicates the type of isotherm to be irreversible ($R_L = 0$), favorable ($0 < R_L < 1$), linear ($R_L = 1$) or unfavorable ($R_L > 1$).

While, the Freundlich isotherm model is expressed as:

$$q_e = K_F C_e^{1/n_F} \tag{6}$$

where K_F and $1/n_F$ are the Freundlich constants, with K_F representing the relative adsorption capacity of the adsorbent and n_F representing the degree of dependence of adsorption on the equilibrium concentration of MB.[39] The experimental data were plots for the non-linearized

Langmuir and Freundlich models (see Fig. 5), and the calculated isotherm constants are summarized in Table 1. The adsorption data plotted of CNF and GO-CNF nanocomposite were well fitted by the Langmuir model (correlation coefficient, r^2 ~0.99) and represent the monolayer adsorption, which is similar to the adsorption mechanism of GO and CNF suspension.[7,24] The maximum adsorptions of CNF, 20%GO-CNF and 20%GO-Fe-CNF nanocomposites acquired from Langmuir were 97.1, 142.3 and 126.6 mg/g, respectively. The adsorption performances for GO-CNF nanocomposites were much lower compared to GO suspension, which are in agreement with recent studies for adsorption of MB for most of the GO-substrates or GO nanocomposites (see Table 2). It can be explained by the interactions of GO with the support materials and reducing the active surface sites for uptaking of adsorbate, which is difficult to avoid.

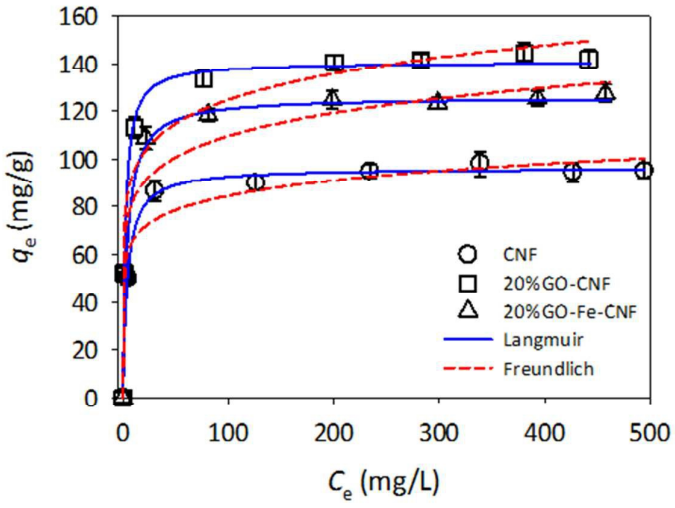

Figure 5 Non-linearized adsorption isotherm of GO-Fe-CNF nanocomposite compared to GO-CNF and CNF (temperature: 20°C; adsorbate dose: 50-600 mg/L)

Table 1 Calculated non-linear isotherm models (Langmuir and Freundlich) for CNF, 20%GO-CNF and 20%GO-Fe-CNF nanocomposites

Adsorbent	Langmuir model				Freundlich model		
	Q_0	b	R_L	r^2	K_F	n	r^2
CNF	97.1	0.15	0.011	0.994	2.65	6.01	0.901
20%GO-CNF	142.3	0.42	0.004	0.997	50.3	6.86	0.904
20%GO-Fe-CNF	126.6	0.25	0.006	0.997	9.15	7.02	0.885

Note, Q_0 (mg/g) = maximum adsorption capacity; b (L/mg) = constant related to adsorption the adsorption energy; R_L = equilibrium parameter; K_F ((mg/g)(L/mg)$^{1/n}$) = relative adsorption capacity; n = degree of dependence of adsorption; r^2 = coefficient correlation

Table 2 Adsorption performances of various GO-substrates for MB removal in recent studies

Adsorbent	Maximum adsorption capacity, Q_0 (mg/g)	Reference
GO	752.1	This work
GO-hydrogel	7.9	Tiwari et al. 2013
GO-polyethersulfone	62.5	Zhang et al. 2013
GO-calcium alginate	181.8	Li et al. 2013
GO-magnetic chitosan	180.8	Fan et al. 2013
20%GO-CNF	142.3	This work
20%GO-Fe-CNF	126.6	This work

3.4 Adsorption with Fenton oxidation

The kinetics of the simultaneous adsorption and Fenton oxidation of MB was plotted in Fig. 6. Since both nanocomposites (20%GO-CNF and 20%GO-Fe-CNF) possess a rapid adsorption for MB removal, at initial stage of simultaneous adsorption-Fenton oxidation process, the performance of the adsorbents are consistent with the single adsorption process (see Fig. S2). As soon as the 20%GO-Fe-CNF achieved adsorption equilibrium at ~30 min, the concentration of MB started to decrease gradually as the H_2O_2 was introduced (see Fig. 6). On the contrary, without Fe(III) loading, no Fenton oxidation occurred on the 20%GO-CNF nanocomposite. Additionally, the adsorption performance of the 20%GO-Fe-CNF was

increased 62.4-86.7% with the assistance of Fenton oxidation. The catalytic activity of 20%GO-Fe-CNF in the presence of H_2O_2 towards MB suggested that the hydroxyl radical of •OH slowly reduced the MB concentration.[40]

Based on the catalytic activity of 20%GO-Fe-CNF on MB, the regeneration of nanocomposites adsorbent was performed by five cycles of MB adsorption and Fenton oxidation with H_2O_2 for 24 hours (see Fig. 7). The regeneration results of the 20%GO-Fe-CNF nanocomposite shows that its adsorption efficiency was decreased after three cycles of the adsorption-oxidation process. The reduction of the adsorption and oxidation performances may be due to the repetitive washing and drying processes, which contributed to the loss of adsorbent and Fe(III) ions. Contrary to 20%GO-CNF, the adsorption performances were reduced drastically after the second cycle of adsorption. The desorption performance of the 20%GO-CNF was lower as compared to neat CNF obtained from our previous study, as a result of strong interaction between MB and GO-CNF.[7] Previous studies on adsorbents loaded with Fe (activated carbon, montmorillonite, etc.) also demonstrated adsorption-oxidation behavior with good adsorption-regeneration cycles of the adsorbent.[37,40,41]

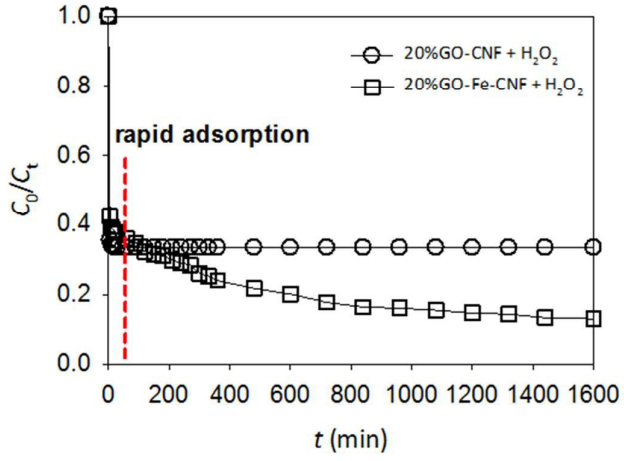

Figure 6 Assisted Fenton oxidation on adsorption of GO-Fe-CNF nanocomposite (a) rapid adsorption phase and (b) Fenton oxidation phase (temperature: 20°C; adsorbate dose: 200 mg/L; H_2O_2: 40 mM)

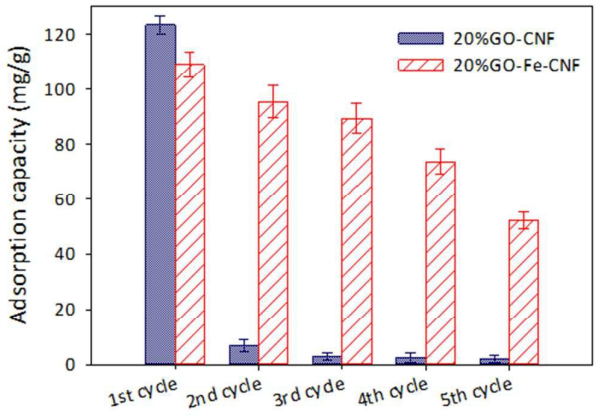

Figure 7 Regeneration of GO/GO-Fe-CNF by desorption (20%GO-CNF) and adsorption-oxidation cycles (20%GO-Fe-CNF) (temperature: 20°C; adsorbate dose: 100 mg/L; H_2O_2: 40 mM)

4. Conclusions

As a conclusion, the produced aerogel nanocomposite composed of GO and CNF demonstrated a rapid adsorption of MB, whilst the adsorption capacity was improved as compared to their stand-alone form. By loading the surface active sites of GO with Fe(III), the removal of MB via adsorption-Fenton oxidation process was twice as effective than the adsorption process. Although it takes a longer time to complete the oxidation phase at a high concentration of MB, this process offered an advantages of regenerating the nanocomposite adsorbent. Compared with the desorption and oxidation processes, the GO and CNF nanocomposite can be regenerated for five cycle adsorption-oxidation processes. Despite the fact that the interactions of GO with the supported material reduced the active surface sites for uptaking of the adsorbate, the recovery of GO after the adsorption is more approachable in wastewater treatments, especially for industry applications.

Acknowledgments

This research was supported by research grants from UKM (DIP-2014-013 & DIP-2015-009) and the Ministry of Higher Education (LRGS/TD/2012/USM-UKM/PT/04).

REFERENCES

1. A. Bhatnagar, W. Hogland, M. Marques and M. Sillanpää, Chem. Eng. J., 2013, 219, 499-511.
2. M. Rafatullah, O. Sulaiman, R. Hashim and A. Ahmad, J. Hazard. Mater., 2010, 177, 70-80.
3. A. Asfaram, M. Ghaedi, S. Hajati, M. Rezaeinejad, A. Goudarzi, and M. K. Purkait, J. Taiwan Inst. Chem. Eng., 2015, 53, 80-91.
4. M. Hua, S. Zhang, B. Pan, W. Zhang, L. Lv and Q. Zhang, J. Hazard. Mater., 2015, 211-212, 317-331.
5. S. Banerjee, R. K. Gautam, A. Jaiswal, M. C. Chattopadhyaya and Y. C. Sharma, RSC Adv., 2015, 5, 14425-14440.
6. A. Shahat, M. R. Awual, M. A. Khaleque, M. Z. Alam, M. Naushad and A. M. S. Chowdhury, 2015, 273, 286-295.
7. C. H. Chan, C. H. Chia, S. Zakaria, M. S. Sajab and S. X. Chin, RSC Adv., 2015, 5, 18204-18212.
8. S. J. Eichhorn, A. Dufresne, M. Aranguren, N. E. Marcovich and J. R. Capadona, J. Mater. Sci., 2010, 45, 1-33.
9. H. P. S. A. Khalil, A. H. Bhat and A. F. I. Yusra, Carbohydr. Polym., 2012, 87, 963-979.
10. G. Siqueira, J. Bras and A. Dufresne, Polym., 2010, 2, 728-765.
11. D. Klemm, F. Kramer, S. Moritz, T. Lindström, M. Ankerfors, D. Gray and A. Dorris, Angewandte Chemie Int. Ed., 2011, 50, 5438-5466.

12. T. Saito, Y. Nishiyama, J.-L. Putaux, M. Vignon and A. Isogai, Biomacromolecules, 2006, 7, 1687-1691.

13. M. Pääkkö, M. Ankerfors, H. Kosonen, A. Nykänen, S. Ahola, M. Österberg, J. Ruokolainen, J. Laine, P. T. Larsson, O. Ikkala and T. Lindström,, Biomacromolecules, 2007, 8, 1934-1941.

14. B. Deepa, E. Abraham, B. M. Cherian, A. Bismarck, J. J. Blaker, L. A. Pothan, A. L. Leao, S. F. D. Souza and M. Kottaisamy, Bioresour. Technol., 2011, 102, 1988-1997.

15. Q. Q. Wang, J. Y. Zhu, R. Gleisner, T. A. Kuster, U. Baxa and S. E. McNeil, Cellulose, 2012, 19, 1631-1643.

16. Q. S. Cheng, Wang and T. G. Rials, Compos. Part A: Appl. Sci. Manuf. Biomacromolecules, 2009, 40, 218-224.

17. K. Dimic-Misic, P. A. C. Gane and J. Paltakari, Ind. Eng. Chem. Res., 2013, 52, 16066-16083.

18. G. Zheng, Y. Cui, E. Karabulut, L. Wågberg, H. Zhu and L. Hu, MRS Bull., 2013, 38, 320-325.

19. N. Ninan, M. Muthiah, I.-K. Park, A. Elain, S. Thomas and Y. Grohens, Carbohydr. Polym., 2013, 98, 877-885.

20. S. Basu and P. Bhattacharyya, Sens. Actuators, B., 2012, 173, 1-21.

21. S.-T. Yang, S. Chen, Y. Chang, A. Cao, Y. Liu and H. Wang, J. Colloid Interface Sci., 2011, 359, 24-29.

22. Y. Liu, J. Zhou, E. Zhu, J. Tang, X. Liu, W. Tang, J. Mater. Chem. C, 2015, 3, 1011-1017.

23. B. Wang, W. Lou, X. Wang and J. Hao, J. Mater. Chem., 2012, 22, 12859-12866.

24. C. H. Chia, N. F. Razali, M. S. Sajab, S. Zakaria, N. M. Huang and H. N. Lim, Sains Malaysiana, 2013, 6, 819-826.

25. X. Zhou and X. Yang, Carbon, 2012, 50, 4566-4572.

26. J. N. Tiwari, K. Mahesh, N. H. Le, K. C. Kemp, R. Timilsina, R. N. Tiwari and K. S. Kim, Carbon, 2013, 56, 173-182.

27. X. Mi, G. Huang, W. Xie, W. Wang, Y. Liu and J. Gao, Carbon, 2012, 50, 4856-4864.

28. B. Yu, J. Xu, J.-H. Liu, S.-T. Yang, J. Luo, Q. Zhou, J. Wan, R. Liao, H. Wang and Y. Liu, J. Environ. Chem. Eng., 2013, 1, 1044-1050.

29. W. M. Algothmi, N. M. Bandaru, Y. Yu, J. G. Shapter and A. V. Ellis, J. Colloid Interface Sci., 2013, 397, 32-38.

30. X. Zhang, C. Cheng, J. Zhao, L. Ma, S. Sun and C. Zhao, Chem. Eng. J., 2013, 215-216, 72-81.

31. L. Fan, C. Luo, M. Sun, X. Li and H. Qiu, Colloids Surf., B, 2013, 103, 523-529.

32. L. Fan, C. Luo, M. Sun, X. Li, F. Lu and H. Qiu, Bioresour. Technol., 2012, 114, 703-706.

33. Y. S. Ho and G. Mckay, Process Biochem., 1999, 34, 451-465.

34. W. Chen, H. Yu, Q. Li, Y. Liu and J. Li, Soft Matter, 2011, 7, 10360-10368.

35. L. Yao, Y. Lu, Y. Wang and L. Hu, Carbon, 2014, 69, 552-562.

36. S. W. Chook, C. H. Chia, S. Zakaria, M. K. Ayob, N. M. Huang, H. M. Neoh and R. Jamal, RSC Adv., 2015, 5, 26263-26268.

37. L. Wang, Y. Yao, Z. Zhang, L. Sun, W. Lu, W. Chen and H. Chen, Chem. Eng. J., 2014, 251, 348-354.

38. I. Langmuir, J. Am. Chem. Soc., 1916, 39, 2221-2295.

39. H. M. F. Freundlich, J. Phys. Chem., 1906, 57, 385-470.

40. Y. Yao, L. Wang, L. Sun, S. Zhu, Z. Huang, Y. Mao, W. Lu and W. Chen, Chem. Eng. Sci., 2013, 101, 424-431.

41. L. Guz, G. Curutchet, R. M. T. Sánchez and R. Candal, J. Environ. Chem. Eng., 2014, 2, 2344-2351.

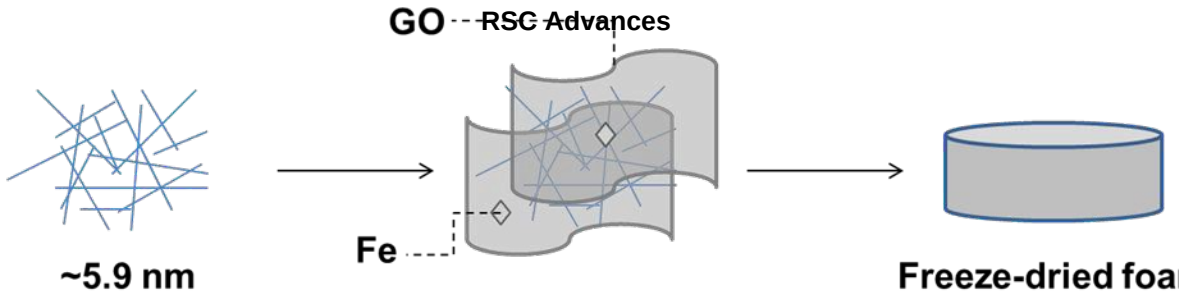

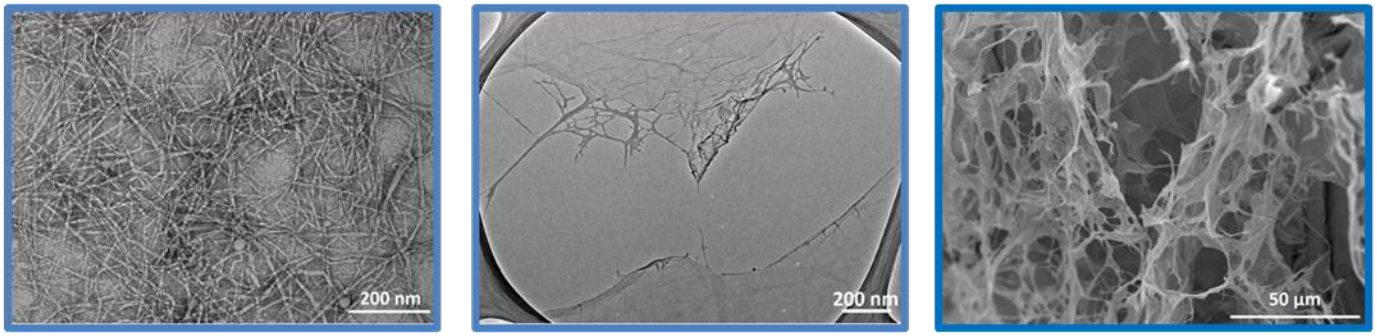

CNF | GOFe-CNF | GOFe-CNF nanocomposite

Dye Removal
(Methylene blue)

Rapid adsorption

+

Fenton oxidation

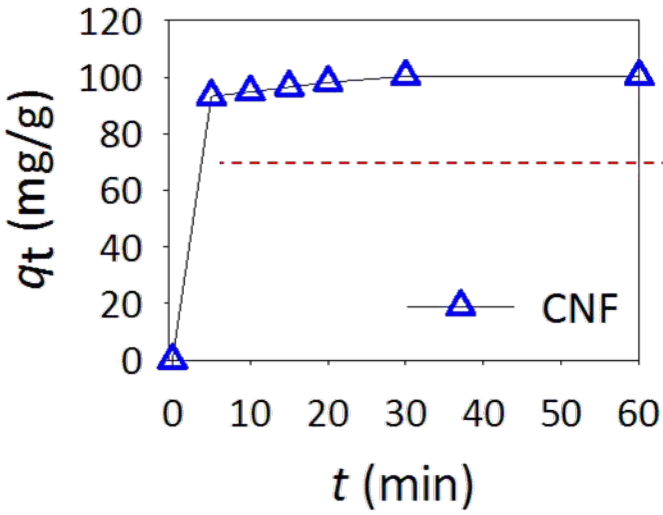

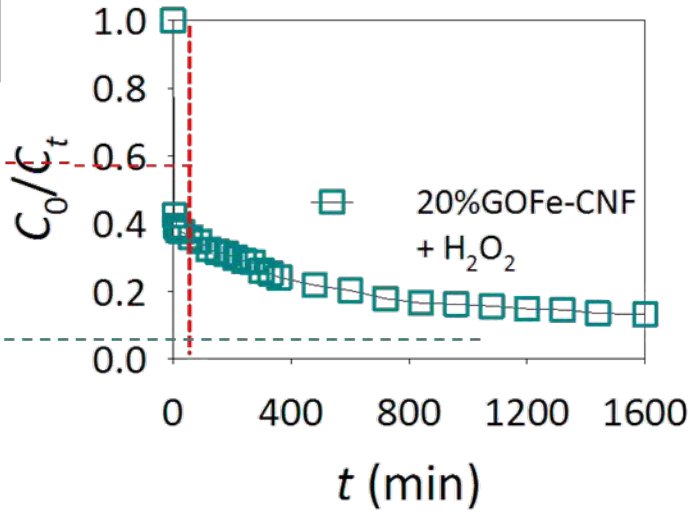

**CNF – Cellulose nanofibrils; GO – Graphene oxide; Fe – Iron*